PROTEINS: Structure, Function, and Genetics 36:484–500 (1999)

Simulating Proton Translocations in Proteins: Probing Proton Transfer Pathways in the *Rhodobacter sphaeroides* Reaction Center

Yuk Yin Sham, Ingo Muegge, and Arieh Warshel*
Chemistry Department, University of Southern California, Los Angeles, California

ABSTRACT **A general method for simulating proton translocations in proteins and for exploring the role of different proton transfer pathways is developed and examined. The method evaluates the rate constants for proton transfer processes using the energetics of the relevant proton configurations. The energies ($\Delta G^{(m)}$) of the different protonation states are evaluated in two steps. First, the semimicroscopic version of the protein dipole Langevin dipole (PDLD/S) method is used to evaluate the intrinsic energy of bringing the protons to their protein sites, when the charges of all protein ionized residues are set to zero. Second, the interactions between the charged groups are evaluated by using a Coulomb's Law with an effective dielectric constant. This approach, which was introduced in an earlier study by one of the authors of the current report, allows for a very fast determination of any $\Delta G^{(m)}$ and for practical evaluation of the time-dependent proton population: That is, the rate constants for proton transfer processes are evaluated by using the corresponding $\Delta G^{(m)}$ values and a Marcus type relationship. These rate constants are then used to construct a master equation, the integration of which by a fourth-order Runge-Kutta method yields the proton population as a function of time. The integration evaluates, 'on the fly,' the changes of the rate constants as a result of the time-dependent changes in charge-charge interaction, and this feature benefits from the fast determination of $\Delta G^{(m)}$. The method is demonstrated in a preliminary study of proton translocation processes in the reaction center of *Rhodobacter sphaeroides*. It is found that proton transfer across water chains involves significant activation barriers and that ionized protein residues probably are involved in the proton transfer pathways. The potential of the present method in analyzing mutation experiments is discussed briefly and illustrated. The present study also examines different views of the nature of proton translocations in proteins. It is shown that such processes are controlled mainly by the electrostatic interaction between the proton site and its surroundings rather than by the local bond rearrangements of water molecules that are involved in the proton pathways. Thus, the overall rate of proton transport frequently is controlled by the highest barrier along the conduction pathway. Proteins 1999;36:484–500.**

Key words: proton pumps; electrostatics; proton transfer in proteins; bioenergetics

INTRODUCTION

Converting light energy to chemical energy is one of the most important ways of providing energy to life processes. Such conversion processes frequently involve a coupling of electron transfer and proton transfer (PT) reactions, resulting in the pumping of protons across membranes.[1] Recent studies have provided detailed three-dimensional structures of proteins, which are involved in proton translocation processes.[2–5] An instructive example is provided by the reaction center of *Rhodobacter sphaeroides* (Fig. 1). Structural studies of this system[2] revealed two branches of water molecules (Fig. 2) that connect directly the solvent-exposed cytoplasmic surface and the secondary quinone (Q_B). One of these branches involves an unbroken chain of 12 water molecules. The other branch, which splits off from the first, consists of two other water molecules and AspL210. It has been suggested[2] that the first water chain may provide the direct PT pathway for the protonation of the Q_B^- anion to Q_BH_2. Conversely, it was proposed based on site-directed mutagenesis studies that the first proton is transferred to Q_B^- through AspL213 and SerL223 and that the second proton is transferred through GluL212 and possibly AspL213.[6] A more recent study[7] based on a new structure[5] has proposed the involvement of three PT pathways.

Although the different proposals for PT pathways are instructive, one still may wonder what governs the rate constant and the pathways for the transfer of protons to the binding site of Q_B. In order to resolve this problem we need more detailed information about the energetics and dynamics of the proton translocation process in reaction centers and other related systems. Here, we attack this problem by developing a computer-simulation approach

Grant sponsor: National Institutes of Health; Grant number: GM40283.
Yuk Yin Sham and Ingo Muegge contributed equally to this article.
Ingo Muegge's present address is Bayer Corporation, 400 Morgan Lane, West Haven, CT 06516.
*Correspondence to: Arieh Warshel, Chemistry Department, University of Southern California, Los Angeles, CA 90089-1062. E-mail: warshel@invitro.usc.edu
Received 22 March 1999; Accepted 6 May 1999

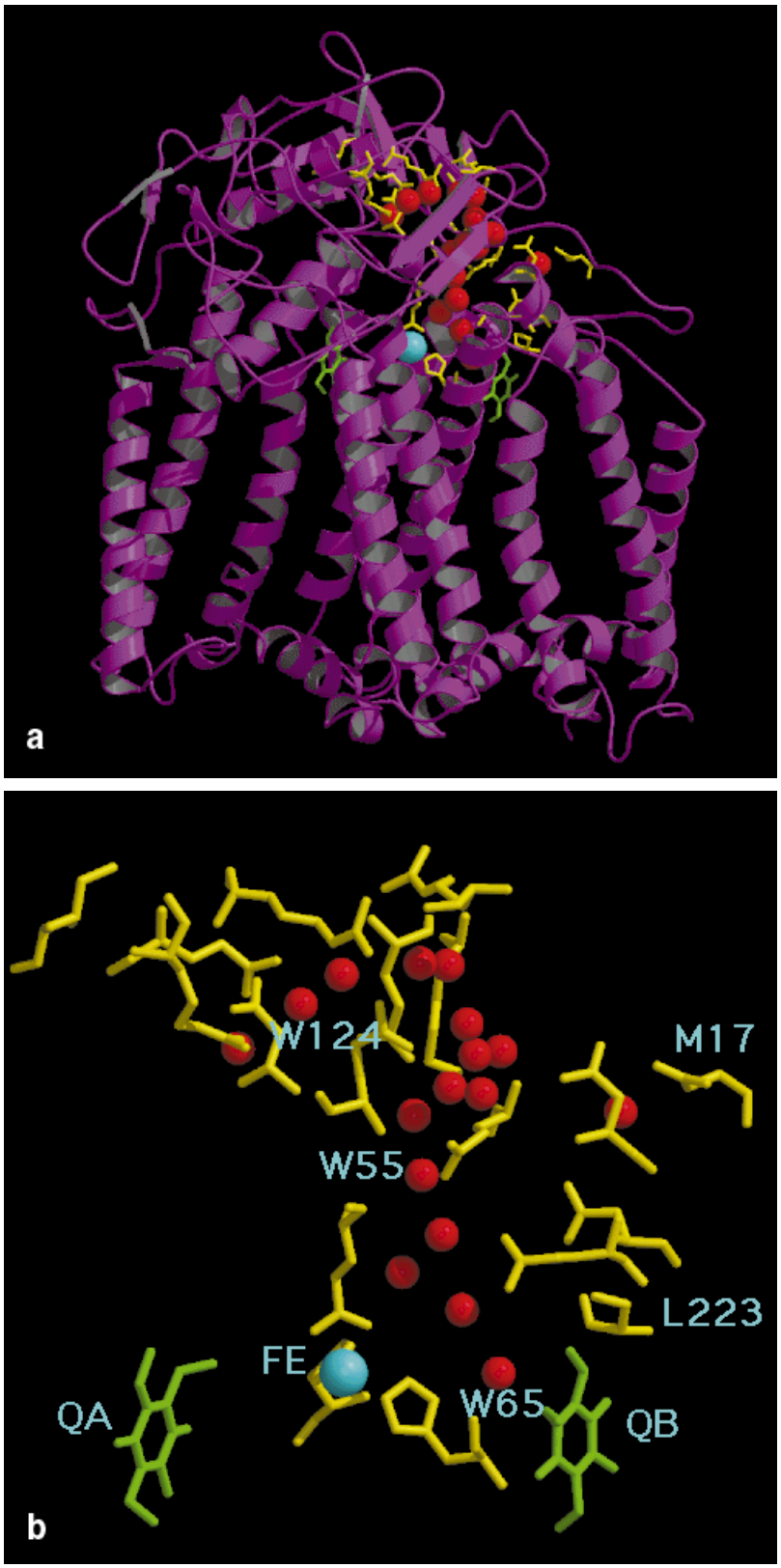

Fig. 1. **a:** The reaction center of *Rhodobacter sphaeroides* with the water molecules leading to the secondary quinone (Q_B). **b:** The region of interest with the ionizable residues (yellow) and water molecules (red) considered in the simulations. The illustrations were created by using MOLSCRIPT.[53]

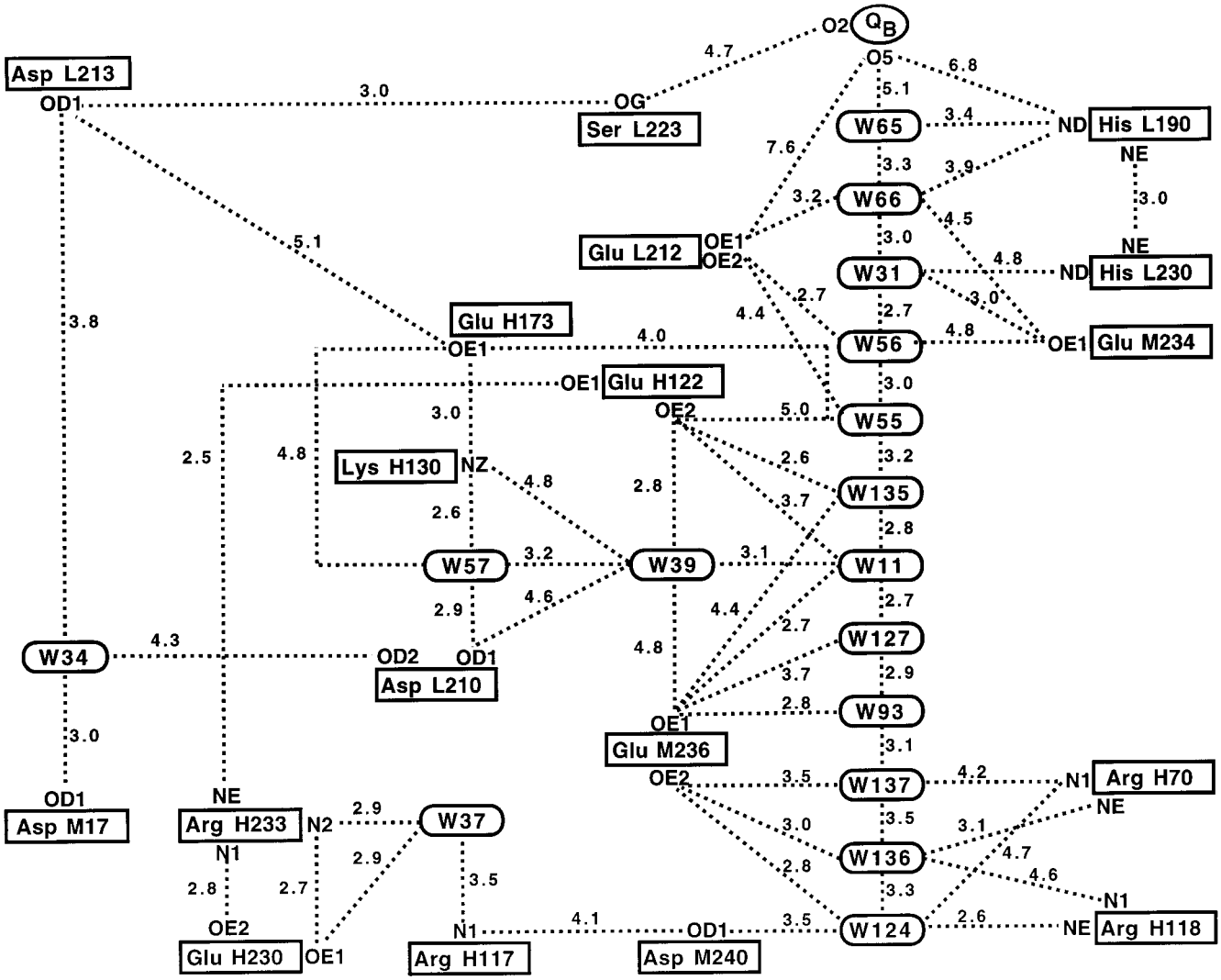

Fig. 2. Schematic description of the groups that can be involved in a proton conductance to Q_B. The numbers near the dotted lines give the corresponding distances in Å. The sequential numbers of the residues are given according to the Protein Data Bank (PDB) notation of the structure (1PCR) of Ermler et al.[2]

aimed at elucidating the details of proton transport processes.

Biological proton conductions can be described by two models with very different natures. A model that has been introduced by Nagel and Morowitz[8] (Fig. 3) is based on the nature of PT in water or ice where the energy of each step is zero. This model involves a chain of proton carriers (e.g., the water molecules shown in Figure 3), which sometimes are connected to an activated proton donor.[9] This model emphasizes the rearrangements of the proton carriers (e.g., bond stretchings) during the proton-hopping process, trying to relate the overall kinetics to the rate constants of the individual steps (which are estimated from the corresponding processes in water or ice). However, no attempt is made to obtain the activation barriers of the individual steps in the protein or to assess the effect of the protein environment on the translocation processes.[9] In fact, Na-

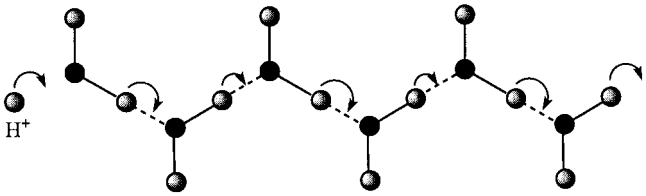

Fig. 3. Nagel's model for transport of an ionic defect (proton) emphasizes bond rearrangement in a chain of proton carriers (e.g., water molecules). The specific picture describes a conductance by a bond-stretching process, but other rearrangements are also considered.[8] This model does not focus on the role of the environment around the proton carriers and on the energetics of the proton transfer (PT) step but, rather, on the kinetic effects of the structural of rearrangements within the chain. These types of rearrangement are important in determining the exact nature of proton transfer in water when the pK_a values of the donor and acceptor are identical but are less important in proteins.

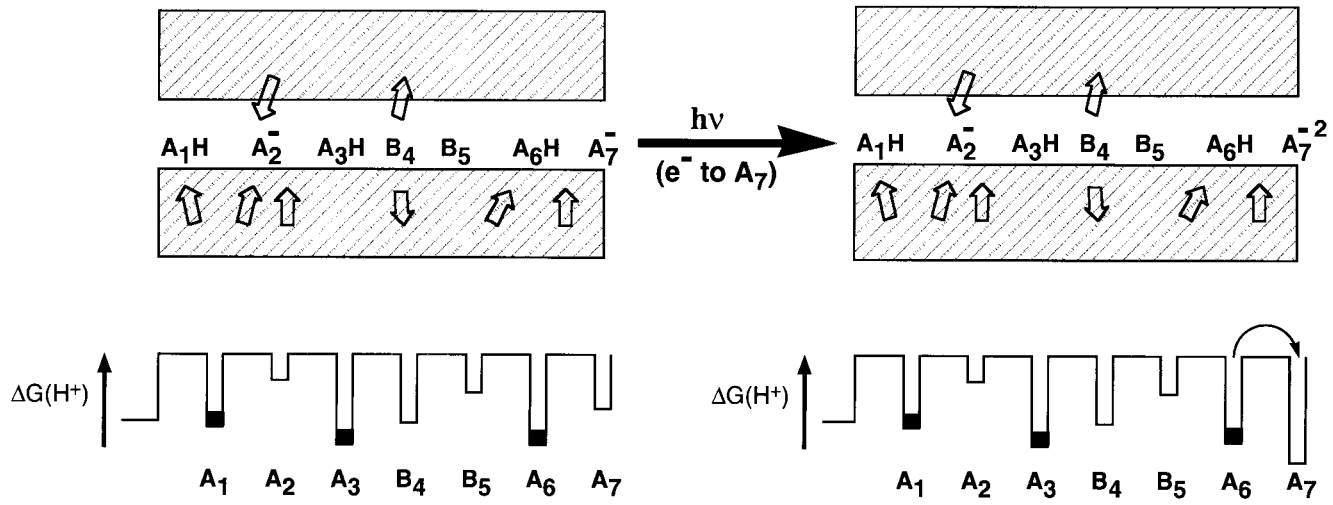

Fig. 4. Warshel's model for proton translocations emphasizes the effect of the environment on the energetics of the ionized forms of the proton carriers rather than the orientation of specific carriers. The original model was constructed for bacteriorhodopsin.[10] It is modified here for proton transport, which is initiated by light-induced electron transfer. This schematic model considers a proton pathway through acids and bases (the bases can be H_2O molecules) embedded in a protein. The protein provides permanent dipoles (i.e., polar groups) that help in stabilizing the charged form of the proton carriers. The energetics of bringing the proton to each proton site is depicted in the lower part of the figure. This energy is determined by the interaction of the charged form of the sites with their surroundings. The sites that are protonated at equilibrium are indicated by black marks. The proton energetics (or the corresponding pK_a values) can be converted to total configuration energy (this is done in Eq. 2; see text) of the reactant and product in each proton transfer step. This and the corresponding reorganization energy allows one to obtain the relevant rate constant. When the donor and acceptor are at a contact distance, the energetics of bringing them to an optimal orientation are usually small in condensed phases. This energy is neglected here relative to the effect of the environment on the site energies. $\Delta G(H^+)$ is the free energy of bringing the proton to the indicated site.

gel and Mille[9] strongly opposed the idea[10] that the energetics of the PT process can be used to obtain the relevant kinetics. This probably reflects unfamiliarity with the Marcus relationship, which is used below (see Materials and Methods) to relate the activation barriers ($\Delta g^{\neq}$) to the free energies (ΔG°) of the corresponding steps. The other model, that was proposed by Warshel[10,11] (Fig. 4), postulates that the most important requirement for proton translocation in proteins is the electrostatic energy of charge formation which is related directly to the values of the acidity constants (the pK_a values) of the different donors and acceptors. This model determines the individual rate constants by using linear free energy relationships (LFER)[11] to relate activation barriers to reaction-free energies. In fact, such an approach was used in the current work.

In considering the two models, the following points should be taken into account: 1) Simulations of PT between water molecules in solution and proteins (see, e.g., Åqvist and Warshel[12] and Warshel[13]) have indicated that the corresponding activation barriers are small ($\approx$1–2 kcal/mol) when the pK_a values of the donor and acceptor are similar and when the donor and acceptor are at a close distance. 2) The effect of structural rearrangement (e.g., bond stretching) of the donor and acceptor on the activation barrier in condensed phase appeared to be small (see Results, below). 3) The activation barriers appeared to depend strongly on pK_a differences between the donor and the acceptor.[11,12] These differences depend drastically on the energies of bringing a proton to the given sites, and these energies are determined by the electrostatic interactions between the sites and their surrounding environment. Thus, once the variation of the electrostatic energies between different sites is more than a few kcal/mol, it can be concluded that the interaction between the protein and the proton sites contributes to the activation barrier much more than the local rearrangement of the donor and acceptors (as long as these molecules are at a contact distance). Despite this argument, it is important to explore the two models in a system that actually is involved in the process of proton translocation.

The current work examines the general issue of the nature of biological proton translocations by considering the proton uptake in the reaction center of *Rhodobacter sphaeroides*. The energetics of the system have been subjected to previous theoretical studies.[7,14–16] However, none of the earlier works explored the kinetics of the proton conduction process. Here, the water chains identified by Ermler et al.[2] are examined as possible PT pathways. The role of local ionizable residues as alternative proton carriers is explored. The detailed nature of proton translocations is studied in a somewhat preliminary way and the main emphasis is placed on introducing a general procedure for studies of biologic proton translocations.

MATERIALS AND METHODS

Our first problem is to evaluate the energetics of PT to different sites of the protein. This is done by considering any relevant, charged configuration, $\Delta G^{(m)}$, relative to the energy of a state in which all of the residues are un-

charged. This free energy is related directly to the pK_a of each proton donor/acceptor at their sites on the protein and is expressed as follows:[10,11,17]

$$\Delta G^{(m)} = \sum_i \{-2.3RTq_i^{(m)}[pK^p_{int,i} - pH] + \tfrac{1}{2}\sum_{i\neq j} W_{ij}q_i^{(m)}q_j^{(m)}\}, \quad (1)$$

where m designates the vector of the charge states of the given configuration [i.e., $m = q_1^{(m)}, q_2^{(m)} \ldots q_n^{(m)}$]. Here, $q_i^{(m)}$ is the actual charge of the ith group at the mth configuration. This can be 0 or −1 for acids and 0 or 1 for bases (where we restrict our formulation to mono ions, although the extension to $|q|>1$ is trivial). The $W_{ij}q_iq_j$ term represents the charge-charge interaction. The intrinsic pK_a (pK_{int}) is the pK_a that the given ionizable group would have if all other ionizable groups were kept at their neutral state (the evaluation of this term is described by Sham et al.[17] Equation 1 also can be expressed in terms of the energy of forming the given configuration in a reference state (in this case, in aqueous solution) at infinite separation of the ions and then transforming it into the protein. This gives[10,18]

$$\begin{aligned}\Delta G^{(m)} &= (\Delta G^{(m)})^w + \sum_i \{-2.3RTq_i^{(m)}[pK^p_{int,i} - pK^w_{a,i}] \\ &\quad + \tfrac{1}{2}\sum_{j\neq i} W_{ij}q_i^{(m)}q_j^{(m)}\} \\ &= \sum_i \{-2.3RTq_i^{(m)}[pK^w_a - pH] \\ &\quad + |q_i^{(m)}|(\Delta\Delta G^{w\to p}_{sol}(q_i^{(m)}))_0 + \tfrac{1}{2}\sum_{j\neq i} W_{ij}q_i^{(m)}q_j^{(m)}|, \end{aligned} \quad (2)$$

where $(\Delta\Delta G^{w\to p}_{sol}(q_i))_0$ represents formally the energy of moving q_i from water to its actual protein site when all other ionizable groups are neutral. In the actual calculation, we also include in $\Delta\Delta G_{sol}$ the solvation of the uncharged form of the given group.[17] $(\Delta G^{(m)})^w$ is the free energy of Equation 1 when all of the residues are in water at infinite separation.

Now, the $\Delta G^{(m)}$ values must be converted to the corresponding energy of protonating the different sites. This can be obtained by[10]

$$\Delta G_{H^+} = \sum_i \Delta G^{(m,i)}_{H^+} = \sum_i (\Delta G^{(m)})_i \times q_i^m, \quad (3)$$

where ΔG_{H^+} is the free energy of the given proton configuration, and $(\Delta G^{(m)})_i$ is the contribution to Equation 2 from its ith term. In more explicit form, we can write

$$\begin{aligned}\Delta G^{(m,i)}_{H^+}(A_i^- \to AH) &= -2.3RT[pK^w_a(A_iH) - pH] \\ &\quad - (\Delta\Delta G^{w\to p}_{sol}(q_i^{(m)}))_0 \\ &\quad - \sum_{j\neq i} W_{ij}q_i^{(m)}\langle q_j^{(m)}\rangle \\ \Delta G^{(m,i)}_{H^+}(B_i \to B_iH^+) &= -2.3RT[pK^w_a(B_iH^+) - pH] \\ &\quad + (\Delta\Delta G^{w\to p}_{sol}(q_i^{(m)}))_0 \\ &\quad + \sum_{j\neq i} W_{ij}q_i^{(m)}\langle q_j^{(m)}\rangle, \end{aligned} \quad (4)$$

where, instead of using the expression for the specific configuration of the q_j values, we consider now the average charge, $\langle q_j\rangle$, at the given pH (see Discussion, below). Applying this approach to H_3O^+ gives

$$\begin{aligned}\Delta G^{(m,i)}_{H^+}(H_2O_i \to H_3O_i^+) &= -2.3RT[pK^w_a(H_3O^+) - pH] \\ &\quad - (\Delta\Delta G^{w\to p}_{sol}(q_i^{(m)}(H_3O^+)))_0 + q_i(H_3O^+)\Sigma_{j\neq i}\langle q_j\rangle W_{ij}. \end{aligned} \quad (5)$$

The average charge distribution of the jth group at a given pH (the $\langle q_j\rangle$) is evaluated by

$$\langle q_j\rangle = \frac{\sum_m q_j^{(m)} \exp\{-\Delta G^{(m)}/RT\}}{\sum_m \exp\{-\Delta G^{(m)}/RT\}}, \quad (6)$$

where $\Delta G^{(m)}$ is approximated by the hybrid approach used by Sham et al.[17] (see also Bashford and Karplus[19] and Yang et al.[20]). This approach evaluates Equation 1 by treating the q_js within a given radius from the ith residue by using a Monte Carlo procedure while replacing the q_j values outside of this radius by $\langle q_j\rangle$ (see Sham et al.[17]). In Equation 4, on the other hand, we use $\langle q_j\rangle$ for all of the residues around q_i. This simplification is essential in order to have a practical treatment for the time-dependent integration described below. In standard pK_a calculations, we use the equivalent of Equation 4 to determine the effect of charge-charge interaction on the apparent pK_a. This is done by looking for the value of the pH at the point where $\langle q_i\rangle = 0.5$ and using this value ($pH = pH_i$) to define the apparent pK_a (pK_{app}) by $pK_{app} = pH_i$. Here, however, we are interested in the protonation state at a fixed pH, and Equation 4 is used accordingly, where all of the $\langle q\rangle$ values corresponds to a single pH.

The calculations of the $\Delta\Delta G_{sol}$ terms were accomplished by using the semimicroscopic version of the protein dipoles Langevin dipoles (PDLD/S) method.[17,21] (see Results, below). The effect of the protein reorganization is considered explicitly in these calculations by using the linear response approximation (LRA) and evaluating the PDLD/S energies for the charged and uncharged states of the relevant residues (for more details, see Sham et al.[17,22]). The interaction term W_{ij} can be calculated in an explicit way (see Sham et al.[17,22]). However, in most cases, we obtain good results by using

$$W_{ij} = 332/(r_{ij}\epsilon_{ij}), \quad (7)$$

where r^{ij} is the distance between the interacting groups, and the value of the effective dielectric constant, ϵ_{ij}, is estimated to be between 25 and 40. The justification of this approximation is discussed in detail elsewhere.[17,22]

In addition to the evaluation of $\Delta G^{(m)}$, the rate constants must be evaluated for the PT processes. Simulations of PT in proteins and solutions can be done in a very effective way by using the empirical valence bond (EVB) method.[13] Such simulations were reported in studies of enzymatic reactions[12] and also include path integral calculations of

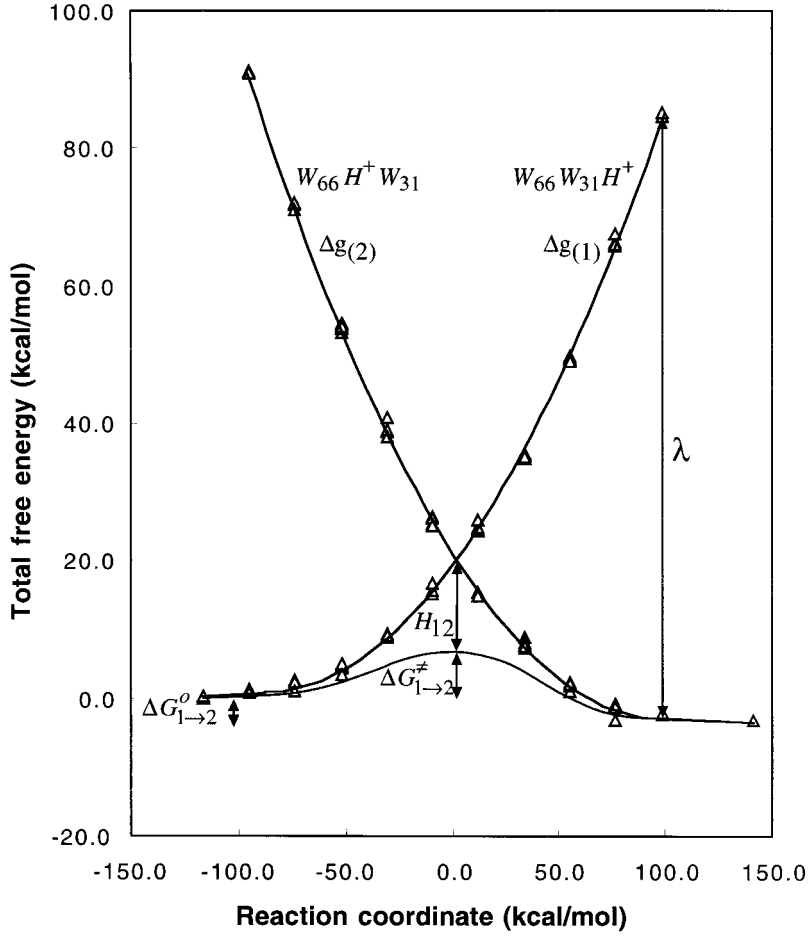

Fig. 5. The relationship between the energetics of proton configurations and the activation barrier of the corresponding PT process. The figure describes the results of an empirical valence bond (EVB) calculation of a proton transfer between W31 and W66 in *Rhodobacter sphaeroides*. The free energy functions $\Delta g_{(1)}$ and $\Delta g_{(2)}$ of the zero-order diabatic states are converted to the ground state free energy function (ΔG) by using the EVB off-diagonal element H_{12}. The figure defines the reorganization energy, λ; the adiabatic activation barriers, $\Delta G^{\neq}_{1\to2}$; and the reaction free energy, $\Delta G^{0}_{1\to2}$. The reaction coordinate is defined in terms of the energy gap between state 1 and state 2. For details, see Warshel[13] and Hwang et al.[26]

proton tunneling.[23] Recent works have used the EVB in a multiconfiguration version (MC-EVB) to study proton conduction in water.[24,25] Despite these advances, it remains impractical to use direct simulations for general studies of proton translocations in proteins, because these processes can be in the μs time range. Thus, we resort here to a master equation treatment. Our method makes use of the $\Delta G^{(m)}$ values for the different proton configurations and the Hwang and Warshel (HW) expression[26], which represents an extension of the Marcus relationship to chemical processes with significant mixing terms. This expression can be written as

$$k_{i\to j} \cong (RT/h)\exp\{-\Delta g^{\neq}_{i\to j}/RT\}$$
$$\Delta g^{\neq}_{i\to j} = (\Delta G^{0}_{i\to j} + \lambda)^2/4\lambda - H_{ij} + H^2_{ij}/(\Delta G^{0}_{i\to j} + \lambda)$$
$$\lambda = \lambda_{int} + \lambda_{sol}, \qquad (8)$$

where λ is the so-called 'solvent reorganization energy,' and it is divided here to the internal contribution of the donor and acceptor, λ_{int}, and to contribution of the surrounding (the solvent), λ_{sol}. $\Delta G^{0}_{i\to j}$ is the free energy of the reaction, and H_{ij} is the off-diagonal term that mixes the two relevant states. A more rigorous expression for $k_{i\to j}$ can be obtained by multiplying the current expression by a transmission factor that can be calculated easily by running downhill trajectories.[13] However, when $\Delta g^{\neq}$ is large (which is the case in the rate-determining steps of the present work), the transmission factor is close to unity, and the approximation of Equation 8 is justified. The nature of the different parameters in Equation 8 is illustrated in Figure 5, which is based on simulations that are considered below (see Results). The parameter ΔG^0 is related directly to the difference between the pK_a of the donor and the acceptor[27], and the changes in ΔG^0 are reflected in the changes of $\Delta g^{\neq}_{i\to j}$ according to Equation 8. When the changes in $\Delta G°$ are small, we obtain a linear relationship between $\Delta g^{\neq}_{i\to j}$ and ΔG^0. More details about this linear free energy relationship (LFER) are given elsewhere.[12,13,26]

Once we evaluate all of the relevant rate constants (the $k_{i\to j}$), we may solve for the time-dependent population of the proton by using the master equation:

$$\frac{\partial[H^+]_i}{\partial t} = \sum_j k_{j\to i}[H^+]_j(t) - \sum_j k_{i\to j}[H^+]_i(t). \qquad (9)$$

This system of ordinary differential equations is solved numerically by using a fourth-order Runge-Kutta method with adaptive, step-size control.[28] Typically, we use an

initial step size of 10–12 seconds. The solution of Equation 9 provides partial occupancy for the migrating proton and therefore leads to non-integer q_i values. The $q_i\langle q_j\rangle W_{ij}$ terms are updated constantly on the fly and, thus, account for the effect of the migrating proton on the pK_as of the ionizable groups participating in the PT process. Note that the $k_{j\rightarrow i}$ depends on the corresponding ΔG^0 values, which are dependent on the protonation states and the $\langle q_j\rangle$ terms. Of course, this dependent is considered in the integration process.

In this work, we assume that the proton distribution found by the hybrid approach of Equation 6 is the distribution that would be obtained by letting the initial system equilibrate. The resulting partial protonation probability of each group is kept constant during the solution of Equation 9, which only involves the single 'mobile' proton that is being injected into our system. The probability of a proton exchanges (when a given group donates its proton to a neighboring group and accepts the mobile proton from another group) is thus simulated by the partial proton distribution of Equation 9. Obviously, there are more realistic ways of writing Equation 9 for a multiple proton model, but they are out of the scope of this work.

The $\Delta\Delta G_{sol}$ values of the crystallographic water molecules and the ionizable residues were evaluated by using the POLARIS program.[21] This was done by using the PDLD/S approach and taking the center of the specific group in each case as the center of its own simulation sphere. This sphere included all of the electroneutral protein groups within a radius of 22 Å as well as Langevin dipoles that represented the water molecules in the empty regions of the simulation system. The sphere was surrounded by a dielectric continuum with $\epsilon = 80$ (for more details, see Sham et al.[17]). The validity and stability of this spherical model was demonstrated repeatedly in early works, including studies of the primary events in reaction centers (see analysis and discussion in Alden et al.[29]). The calculation involved an LRA averaging[17] of the PDLD/S energies over protein configurations generated by molecular dynamics (MD) simulations of the charged and the uncharged states. These simulations involved the ENZYMIX force field[21] and the surface constraint all-atom solvent (SCAAS) model.[21,30] It is possible that more reliable results could have been obtained by modeling the membrane regions using a low dielectric grid of induced dipoles, as was done in our early studies.[29] However, here, we deal mainly with groups that are close to internal water molecules or to the bulk solvent, and these regions tend to compensate for the loss of solvation due to the membrane region by increasing their own contributions.

The calculations represented the ionizable residues as well as the rest of the protein atoms by the standard ENZYMIX charges.[21] The Fe^{+2} ion was modeled as a +1 ion where the extra positive charge was spread equally on the two histidine ligands. The quinone charges were taken from QCFF/PI calculations.[31] The distance dependence of the $k_{j\rightarrow i}$ values was calculated at the first step of the integration. This was done by starting from a Protein Data Bank (PDB) file that contained all of the atoms that may accept the proton (e.g., NH1 and NH2 for ARG, OG for SER, OD1 and OD2 for ASP, etc.). The coupling between residue pairs was then evaluated by taking the minimum distance between the participating atoms in the given pair. The calculated coupling was kept constant during the integration. The $W_{ij}q_iq_j$ term, however, was reevaluated at each step of the integration of Equation 9 using the above PDB.

RESULTS

Energetics of Different PT Pathways

In the present study, the water molecules and ionizable residues shown in Figure 2 are considered to be feasible candidates for PT in *Rhodobacter sphaeroides* (Fig. 1). The initial basis for this selection was based on the earlier studies by Ermler et al.[2] (see their Fig. 11). However, only ionizable groups in which the side chains are within 5 Å from the water molecules in the water chain are considered to be elements of the proton-conduction process. This excludes AspH174, ArgH181, and GluM230 from the master equation. On the basis of site-directed mutagenesis studies,[6] SerL223 and AspL213 are included in our work.

The first step in our analysis involved the calculations of the energetics of protonating different internal water molecules that may be involved in proton transport pathways. The pK_a values of the corresponding H_3O^+ ions and the nearby ionizable residues are given in Tables I and II. A quantitative estimate of the energetics of transferring a proton across a water chain requires both of the $\Delta\Delta G$ values and the actual activation barriers between adjacent sites. Although we estimated the activation barriers in our time-dependent calculations (see below), we also generated a qualitative picture by considering the relevant $\Delta\Delta G$ values. In doing so, we took advantage of the observation that the difference between the activation barriers and exothermicities is rather small as long as the donor and acceptor are at a contact distance. This fact emerges from experimental studies[32] and from many EVB simulations of PT in solution and proteins.[12] With this in mind, we used the calculated $\Delta\Delta G$ values in Figure 6 to generate a qualitative free energy profile for transferring a proton across a water chain at pH 7.0. It is clear from the figure that the energetics of conducting the proton along the water chain depends in a substantial way on the local field from the surrounding protein. For example, the free energy of transferring a proton from W11 to W55 is ~10 kcal/mol. Finding such a large $\Delta\Delta G$ means that the protein environment controls the PT process. The implication of this finding are discussed in more detail below.

Figure 2 shows that there are several alternative pathways for the proton conduction process. These include the original water chain (12 water molecules) and various chains in which the water molecules are bridged by ionizable residues of the protein. The actual energetics of protonating these residues depends, of course, on their environment. To explore this issue, we constructed the relevant free energy diagram for the pathways that involves 12 water molecules and nearby ionizable residues. It can be seen from the corresponding energy profile (Fig.

TABLE I. Calculated Protonation Free Energies and Related Quantities for Water Molecules in the Reaction Center of *Rhodobacter sphaeroides*[†]

Residue	$(\Delta\Delta G_{sol}^{w\rightarrow p})_o$[a]	pK_{int}[b]	ΔG_{int} (pH 7.0)[c]	ΔG_{qq} (pH 7.0)[d]	ΔG_{eff} (pH 7.0)[e]	$\Delta\Delta G$ (pH 7.0)[f]
wat11	14.1	−11.9	14.1	−5.1	21.0	9.0
wat31	14.7	−12.3	14.7	−5.7	21.0	9.0
wat34	13.4	−11.4	13.4	−4.9	20.5	8.5
wat37	13.1	−11.2	13.1	−1.6	23.5	11.4
wat39	16.4	−13.6	16.4	−5.3	23.1	11.1
wat55	20.3	−16.4	20.3	−5.3	27.0	15.0
wat56	14.8	−12.4	14.8	−6.2	20.6	8.6
wat57	20.3	−16.4	20.3	−3.9	28.4	16.4
wat65	17.2	−14.1	17.2	−4.8	24.3	12.3
wat66	13.4	−11.4	13.4	−5.6	19.8	7.8
wat93	13.9	−11.8	13.9	−4.4	21.5	9.5
wat124	13.2	−11.2	13.2	−2.9	22.3	10.3
wat127	12.6	−10.8	12.6	−3.4	21.1	9.1
wat135	17.0	−14.0	17.0	−5.6	23.4	11.4
wat136	12.9	−11.0	12.9	−1.6	23.3	11.3
wat137	16.1	−13.3	16.1	−3.9	24.2	12.2

[†]Calculated PDLD/S-LRA energies using the crystal structure of the *Rhodobacter sphaeroides* reaction center (1PCR)[2] with MD-LRA treatment and $\epsilon_p = 4$. All free energies are given in kcal/mol, whereas the calculated intrinsic pK_a is given in pK_a units.

[a]Calculated change in solvation energy of the ionized state of the indicated group in its site in the reaction center relative to the corresponding energy in bulk water.

[b]Calculated intrinsic pK_as of crystallographic water of *Rhodobacter sphaeroides*.

[c]Calculated free energy of protonating crystallographic water inside the *Rhodobacter sphaeroides* reaction center (in the absence of other ionized groups) by a cytoplasmic hydroxonium ion [$\Delta G(H_3O^+_{(w)} + H_2O_{(p)} \rightarrow H_2O_{(w)} + H_3O^+_{(p)}$] at pH 7.0 (the first two terms of Eq. 5).

[d]Calculated contributions to the free energy of protonation of the indicated group from its charge-charge interaction with all other ionizable residues, with their average charges at pH 7.0 (this is the W_{ij} term of Eq. 4). The calculations are done with $\epsilon_{ij} = 40$.

[e]Calculated free energy of deprotonating a hydroxonium ion inside the *Rhodobacter sphaeroides* reaction center (in the presence of other ionizable groups) at pH 7.0.

[f]Calculated free energy of protonating crystallographic water inside the *Rhodobacter sphaeroides* reaction center (in the presence of other ionizable groups) by a cytoplasmic hydroxonium ion at pH 7.0, relative to the corresponding free energy of protonating a water molecule in the bulk.

7) that the ionized residues provide very low energy sites for the proton. Thus, it is likely that some of these residues are involved in the PT process. To explore the actual role of these ionizable residues requires the determination of the kinetics of the proton-conductance process. Such a study is described in the next section. It should be clarified at this point that the free energy profile of Figure 7 is evaluated for an assumed pathway without any time dependent study. Thus the actual pathway (or pathways) might be quite different than that chosen here for the purposes of illustration.

At this point, it is instructive to examine what are the most important contributions to the activation barriers ($\Delta g^{\neq}$) for PT steps along a water chain. In addressing this question, we are interested mainly in the nature of $\Delta g^{\neq}$ inside proteins, because $\Delta g^{\neq}$ is very small in bulk water.[24,25] Now, the internal rearrangements of the donor and acceptor (which are the main feature of Nagel's model[9]) can influence $\Delta g^{\neq}$ through the corresponding contributions to H_{ij} and λ_{int} of Equation 8. Thus, one may assume that the internal rearrangements can be drastically different in proteins and in water, and this would contribute to the corresponding difference in $\Delta g^{\neq}$. However, it usually costs very little to bring the donor and acceptor to the same relative orientation and distance that they have in water. To demonstrate this point, we write the activation barrier as

$$\Delta g^{\neq}(r_{ij})_{i\rightarrow j} = w(r_{ij} \rightarrow r^{\circ}_{ij}) + \Delta g^{\neq}(r^{\circ}_{ij})_{i\rightarrow j}, \qquad (10)$$

where r_{ij} is the actual distance between the donor and acceptor, and r°_{ij} is the distance for optimal PT, where $\Delta g^{\neq}$ is the smallest. The term $w(r_{ij} \rightarrow r^{\circ}_{ij})$ is the work of moving the donor and acceptor from r_{ij} to r°_{ij}. This term is related to the well known 'w' term in Marcus theory (e.g. see ref. 33). Here, we evaluated the $w(r_{ij} \rightarrow r^{\circ}_{ij})$ for W66 and W31 by calculating the corresponding potential of mean force (PMF) for changing r_{ij} from 4.5 Å to 2.7 Å. The calculations were done by using a free energy perturbation (FEP)/umbrella sampling approach with a distance constraint that changed gradually from 5 Å to 2.5 Å in 11 mapping steps, with a total simulation time of 50 ps. The MD simulations were done with 1 fs time steps at 300 K. Similar results were obtained for the pair W31 and W55, in which it cost only 0.5 kcal/mol to change the distance from 4 Å to 2.7 Å. The generality of these results can be rationalized easily by realizing that, for each donor-acceptor pair, there is one neutral water molecule that usually can be displaced within the protein at a relatively small cost. On the other hand, it is quite easy to change

TABLE II. Calculated Protonation Free Energies and Related Quantities for Relevant Ionizable Groups in the Reaction Center of *Rhodobacter sphaeroides*†

Residue	$(\Delta\Delta G_{sol}^{w\rightarrow p})_o$[a]	pK_{int}[b]	ΔG_{int} (pH 7.0)[c]	ΔG_{qq} (pH 7.0)[d]	ΔG_{eff} (pH 7.0)[e]	$\Delta\Delta G$ (pH 7.0)[f]
argH117	13.8	2.5	−5.8	−5.9	0.4	−11.6
argH118	6.7	7.6	−12.9	−3.3	−4.1	−16.2
argH70	12.7	3.3	−6.9	−3.1	2.0	−10.0
argM233	11.5	4.1	−8.1	−6.0	−2.0	−14.0
aspL210	1.1	4.8	−9.0	1.9	1.2	−10.8
aspL213	3.7	6.6	−11.5	1.8	−1.3	−13.3
aspM17	1.4	5.0	−9.2	−1.0	3.8	−8.2
aspM240	4.5	7.3	−12.4	1.2	−1.6	−13.6
gluH122	3.0	6.6	−11.4	2.1	−1.5	−13.5
gluH173	1.4	5.4	−9.8	1.3	0.8	−11.2
gluH230	4.3	7.5	−12.8	0.3	−1.0	−13.0
gluL212	5.9	8.7	−14.3	2.3	−4.6	−16.6
gluM234	11.9	13.0	−20.3	−1.1	−7.2	−19.2
gluM236	1.6	5.6	−10.0	1.3	0.7	−11.3
hisL190	8.6	0.3	−2.8	8.5	17.7	5.7
hisL230	6.3	1.9	−5.0	−3.7	3.3	−8.7
lysH130	14.6	−0.2	−2.0	−7.3	2.7	−9.3
serL223	4.3	18.1	−27.3	2.3	−17.6	−29.6
Q_B	3.2	7.2	−12.3	0.6	−0.9	−12.9

†Calculated PDLD/S-LRA results using the crystal structure of the *Rhodobacter sphaeroides* reaction center (1PCR).[2] The results were obtained with MD-LRA treatment and $\epsilon_p = 4$. All free energies are given in kcal/mol, and the calculated intrinsic pK_a is given in pK_a units.

[a]Calculated change in solvation energy of the ionize state of the indicated group in its site in the reaction center relative to the corresponding energy in bulk water (see Eq. 2).

[b]Calculated intrinsic pK_as of the indicated ionizable residues of *Rhodobacter sphaeroides*.

[c]Calculated free energy of protonating relevant ionizable residues inside the *Rhodobacter sphaeroides* reaction center (in the absence of other ionized groups) by a cytoplasmic hydroxonium ion at pH 7.0 ($\Delta G(H_3O^+_{(w)} + A^-_{(p)} \rightarrow H_2O_{(w)} + AH_{(p)}$ for acids, and $\Delta G(H_3O^+_{(w)} + B_{(p)} \rightarrow H_2O_{(w)} + BH^+_{(p)}$ for bases; Eq. 4 without the W_{ij} term).

[d]Calculated charge-charge interactions between the ionized state of the indicated group with all other ionizable residues with their average charges at pH 7.0 (this is the W_{ij} term of Eq. 4). The calculations are done with $\epsilon_{ij} = 40$.

[e]Calculated free energy of deprotonating an acid (or a charged base) inside the *Rhodobacter sphaeroides* reaction center (in the presence of other ionizable groups) at pH 7.0 (see Eq. 4).

[f]Calculated free energy of protonating the indicated group inside the *Rhodobacter sphaeroides* reaction center (in the presence of other ionizable groups) relative to the corresponding energy of protonating water molecule in water.

$\Delta g^{\neq}$ by changing the ΔG_0 and λ_{sol} of Equation 8, as established repeatedly in EVB studies (e.g., ref. 12) and in the current work. Thus, we conclude that large changes in $\Delta g^{\neq}$, for donor and acceptor pairs that are at reasonable distances, are due to the environment around the pair (see, e.g., Fig. 7) and not to the relative orientation within the pair.

It should be mentioned here that the seemingly related picture that emerges from gas-phase, ab initio calculations is not directly relevant to the situation in solutions and proteins. That is, gas-phase, ab initio calculations of PT between water molecules[34,35] emphasize the importance of structural deformations of the donor-acceptor complex. However, these gas-phase effects (which also are reproduced accurately by gas-phase EVB calculations) are not as relevant to the energetics along the actual least energy path and the corresponding activation barrier in solutions and proteins. First, energy contributions from structural rearrangements are compensated for partially by the response of the surrounding environment. Second, as discussed above, it is very easy to move the donor-acceptor complex from a deformed structure to the optimal orientation in which $\Delta g^{\neq}$ reaches its lowest value. Finally, and quite obviously, gas-phase calculations of a PT across several water molecules miss the effect of the surrounding protein on the relevant ΔG^0.

Time Dependence of the PT Process

Using Equations 2, 3, 7, and 8 allows us to evaluate the $\Delta G^0_{i\rightarrow j}$ and $k_{i\rightarrow j}$ for a PT between any donor-acceptor pair. The evaluation of the rate constants only requires the knowledge of λ_{ij} and H_{ij}. Here, we assume that the distance dependence of λ_{sol} follows the continuum relationship[36]

$$(\lambda_{ij})_{sol} = (\lambda^0_{ij})_{sol}\left(1 - \frac{a_i + a_j}{2r_{ij}}\right)$$

$$(\lambda_{ij})_{int} = (\lambda_{ij}(r_{ij} = 3))_{int}\left(\frac{(\lambda_{ij})_{sol}}{(\lambda_{ij}(r_{ij} = 3))_{sol}}\right), \qquad (11)$$

where $(\lambda_{ij})_{sol}$ is the solvent reorganization energy for the PT process between the donor and acceptor at infinite separation, r_{ij} is the distance between the donor and the

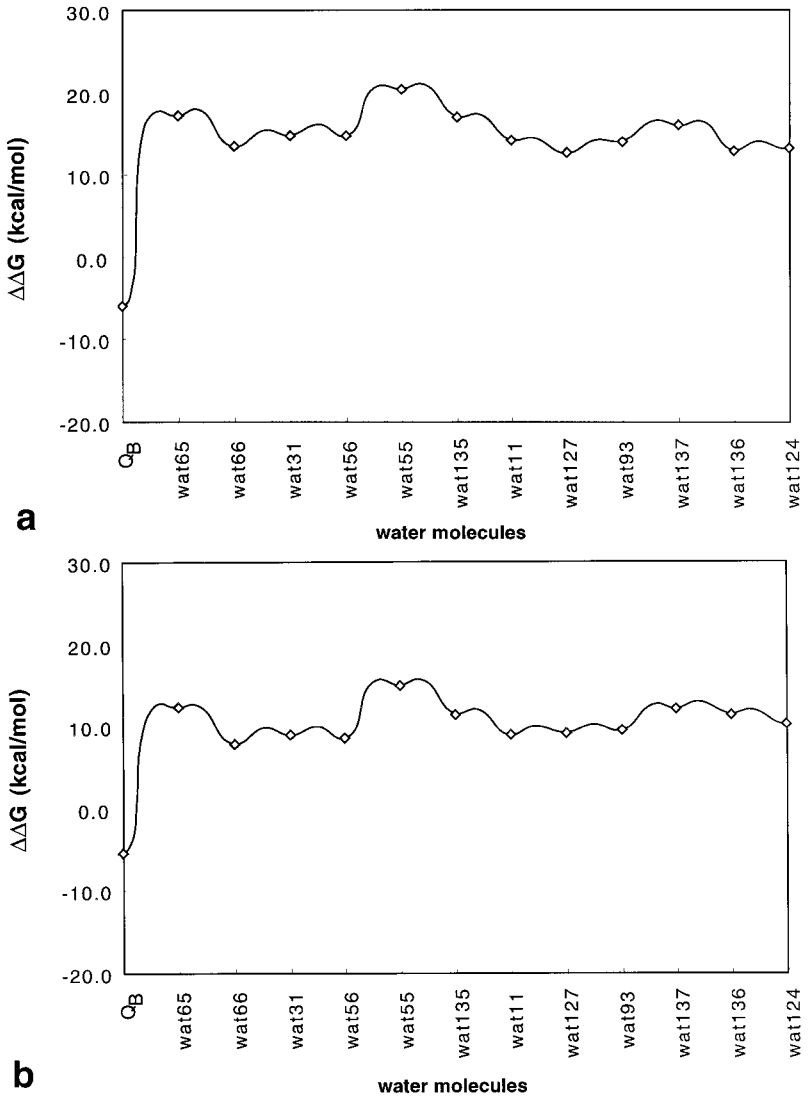

Fig. 6. The free energy profile for proton conductance along the indicated chain of water molecules. **a:** The intrinsic free energy without the effect of other protein ionized residues. **b:** The free energy profile that includes the electrostatic effect of the protein ionized groups. The minima of the free energy profile are determined by the corresponding ΔΔG values (diamonds) The barriers between adjacent minima can be determined by using Equation 8; however, they are drawn here schematically.

acceptor, and a_i and a_j are the Born's radii of the donor and acceptor. In writing Equation 11, we approximate $(\lambda_{ij})_{int}$ by using the same distance dependence as that of $(\lambda_{ij})_{sol}$. A more rigorous approach clearly can be used, but this is not justified in the present treatment, because it does not consider distance fluctuations and because, as discussed above, donors and acceptors at an intermediate distance can be brought easily to an optimal distance.

To determine the parameter λ^0, we performed EVB simulations of PT between the two water molecules (W31 and W66 whose separation, r_{ij}, is 3 Å). The EVB calculations involved a free energy perturbation/umbrella sampling procedure.[13,26] These calculations were performed by using the ENZYMIX program.[21] The simulations were done by using a 22-Å SCAAS simulation sphere with the local reaction field (LRF) long-range treatment.[37] The data collection involved 15-ps equilibration and 30-ps FEP calculations with 11 windows. The MD simulations were done with 1-fs time steps at 300 K. The diabatic surfaces obtained by the simulations as well as the corresponding adiabatic surface are depicted in Figure 5, which shows that the reorganization energy (λ) is ≈80 kcal/mol. We also find that $(\lambda_{ij})_{sol} \approx 40$ kcal/mol. Taking the parameters a_i and a_j as the Born's radius that reproduces the solvation energy of H_3O^+ ($a \cong 1.3$ Å), we obtain $\lambda^0_{sol} \approx 74$ kcal/mol. H_{ij} is approximated by the regular EVB approximation $H_{ij} = A \exp(-\mu(r - r_0))$. The parameters A and μ were retained by EVB studies of PT reactions and the values used $A = 20$ kcal/mol, $\mu = 2$ Å^{-1}, and $r_0 = 3.0$ Å.

The solution of Equation 9 requires one to set the proper initial conditions. At present, despite a great deal of work,[7,38–51] it is not entirely clear when PT occurs, because

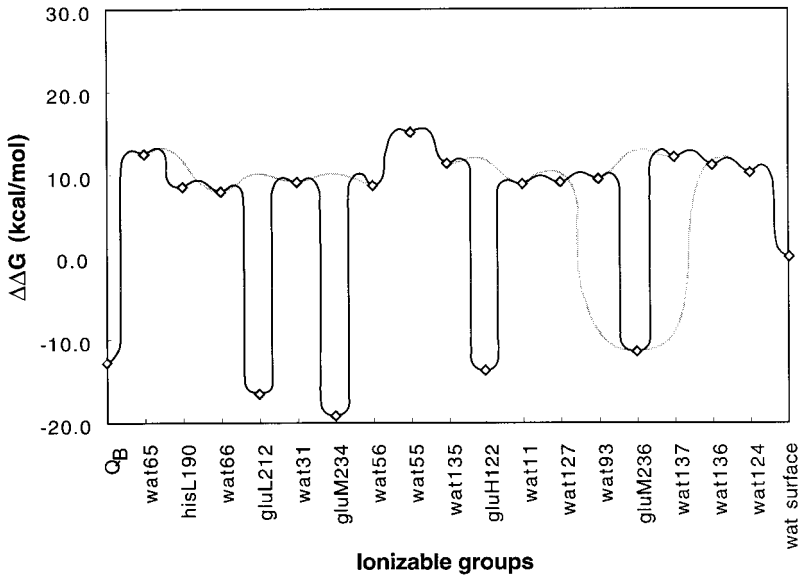

Fig. 7. A free energy profile for a proton conductance that involves both water molecules and protein residues. This profile includes the effect of the interaction between ionized residues. An alternative profile that keeps some sites is also indicated.

this process is not thought to be rate limiting. It is known that the absorption of the first photon of light leads to the formation of $Q_A^-Q_B^-$ in ≈200 ps and that electron transfer from Q_A^- to Q_B occurs in ≈100 μs, leading to the formation of $Q_A^-Q_B$.[46] The absorption of the second photon leads to the formation of $Q_A^-Q_B^-$ in ≈200 ps and then to a proton-coupled electron transfer from Q_A^- to Q_B^- in ≈1 ms. However, the nature of this step is less clear; it may involve a stepwise process[46]

$$Q_A^-Q_B^- + H^+ \rightarrow Q_A^-Q_BH \rightarrow Q_A(Q_BH)^-, \quad (12)$$

or a concerted single-step process

$$Q_A^-Q_B^- + H^+ \rightarrow Q_A(Q_BH)^-, \quad (13)$$

or an even less likely mechanism

$$Q_AQ_B^- + e^- + H^+ \rightarrow Q_AQ_B^= + H^+ \rightarrow Q_A(Q_BH)^-. \quad (14)$$

Careful studies of these options[46] could not determine conclusively the actual mechanism, and it can be concluded only that the PT must be faster or equal to the overall rate of ≈1 msec. Trying to be consistent with the known information, we have to start from $Q_AQ_B^-$ and to trigger the PT process by forming $Q_A^-Q_B^-$. In doing so, we assume that Q_B^- reaches some form of equilibration in the configuration found by the X-ray structure. Here, it might have been better to use more recent structural studies,[5] in which Q_B^- is located at its binding pocket. However, the present study tries to take the X-ray structure of Ermler et al.[2] at its face value and leaves more careful studies of the structural dependence of the calculations to subsequent studies. At any rate, we start by equilibrating the protonation states at the X-ray structure of $Q_AQ_B^-$ (in this process, we find 70% Q_B^- and 30% Q_BH). Next, we simulate the formation of $Q_A^-Q_B^-$ (and of a possible further relaxation of the system following previous steps) by increasing the pK_a of Q_B^-. This is done by reducing the free energy of the process $Q_B^- + H^+ \rightarrow Q_BH$ by 3.4 kcal/mol. In evaluating the resulting change in proton population, we are not trying to distinguish between the mechanisms of Equations 12–14. However, this could have been done by using the EVB formulation for both the electron transfer and the PT processes. The resulting Marcus-type approach is expected to provide results similar to those obtained by simulating the first step of Equation 12; however, actual study of this issue is beyond the scope of this paper.

In studying proton transport, it would be interesting to explore two mechanisms. The first mechanism involves a PT from the bulk to Q_B^-. In this mechanism, we consider the time of diffusion of proton from the bulk to a surface molecule and then a translocation of the proton from the surface molecule to Q_B^-. The second mechanism involves a donation of a proton to Q_B^- from an internal group that is already protonated in the resting state. The transfer of this proton is followed by a reprotonation from the bulk solvent. Here, we will focus mainly on the first mechanism and only examine some aspects of the second.

The study of PT from the bulk through a surface molecule to Q_B^- was done by simulations that considered the diffusion time of H^+ to a surface molecule ($W_{surface}$) that is located near W124. The diffusion time was estimated roughly under the assumption that the hydronium cation diffuses with the same diffusion constant as water molecules in bulk water. Considering the concentration of hydronium cations in water at pH 7.0, one finds that the average distance between two hydronium cations is ≈1,100 Å. By using a diffusion constant of ≈0.2 Å²/ps, the average time for an ion to reach the starting position of a second hydronium cations is ≈20 μsec. Here, we assume that the average distance between a water molecule at the protein surface (e.g., $W_{surface}$) and a bulk hydronium ion is not larger than the distance estimated above [the average

distance between a surface water molecule and a hydronium ion in the bulk would be only half of the interhydronium distance (≈550 Å), and the diffusion time would only be ≈4 μsec]. From this coarse consideration, we estimate that the time it takes for a hydronium cation in the bulk to reach $W_{surface}$ is <20 μsec. Thus, we start the actual simulations at t = 20 μsec, with a change of the free energy of a proton on Q_B^- from −8.6 kcal/mol to −12 kcal/mol (to simulate the process $Q_AQ_B^- + e^- \rightarrow Q_A^-Q_B^-$) and with a placement of a full proton on $W_{surface}$. Starting with these initial conditions, we follow the proton occupancy on different groups as a function of time along the possible pathways to Q_B.

The change of the participating residues, as discussed above (see Materials and Methods), results in changes of the pK_a values of the residues along the PT pathway. This is accounted for in the simulations through the terms $q_iq_jW_{ij}$, which are calculated on the fly during the evaluation of the derivatives of the proton occupancy as a function of time. The simulations involved the solution of Equation 9, as described in Materials and Methods. The proton migration process was followed for 20 μsec per run for a total of 2×10^7 steps. Such a calculation took 8 hours per run on an R10000 SGI workstation. The simulated, time-dependent proton population is shown in Figure 8a. The overall result is a transfer of the proton from the surface water molecule to Q_B and to a some other residues. The transfer time is ≈40 μsec, and this time is consistent with the assumption that the transfer of the first proton is faster than the rate of transfer of the second electron (≈1 msec at pH 7.5[46]). Figure 8a shows that there is also a partial probability that the proton will be transferred to ArgH117, Glu M236, GluH173, AspL210, and ArgH70. Most of these groups are not included in the free energy profile of Figure 7. This is due to the fact that the figure represents the energetics along an arbitrarily selected path. This path does not includes the nonproductive branches (such as the one to GluH173) that do not lead to Q_B but that still can lead the proton to temporary traps. Unfortunately, the populations presented in Figure 8a do not tell us about the proton pathways. That is, the rate-limiting transfer of the proton through the high-energy acceptors is a very rare event that cannot be detected simply by monitoring the very small probability of being on these acceptors.

The proton translocation in *Rhodobacter sphaeroides* is thought to involve several pathways,[7] and one of these pathways was proposed to involve AspM17 as an entry point.[7] To explore this suggestion, we started a simulation from a surface proton near AspM17 rather than near W124. The results of this simulation are shown in Figure 8b. The population of Q_B and other groups is somewhat slower than that of Figure 8a. This indicates that the initial barriers are different in the two processes. However, the overall picture after 20 μsec is similar, indicating that the rate-determining barrier is similar. A more complete analysis of the difference between the two pathway would require the deletion of different bridging molecules, and it is out of the scope of the present work. Nevertheless, the present analysis indicates that both pathways are equally viable.

Figure 2 and Table II can be used to examine feasible pathways in a tentative way. This is limited, of course, by the protein structure used. For example, with the structure of Ermler et al.[2] (which is the basis for Fig. 2), one can exclude a pathway in which the proton migrates to Q_B through AspL210, W34, AspL213, and SerL223. AspL213 is protonated in the present model, and the process of a simultaneous PT from this group to SerL223 and acceptance of a proton from W34 is not captured by the present master equation. Nevertheless, the transfer of a proton by a double protonation of AspL213 remains feasible. However, SerL223 is at a distance of almost 5 Å to the proton acceptors on Q_B, and this excludes a PT from SerL223 to Q_B. To be certain about this point, we performed an additional simulation that reduced the free energy of the protonated SerL223 to 10 kcal/mol, making it an excellent acceptor for a second proton. However, this simulation did not change the proton population at all, leaving it the same as in Figure 8a. This indicates that SerL223 is not a part of any branch in the present model. Of course, using other X-ray structures as well as considering distance fluctuations could make the residue a part of a proton pathway.

We were also interested in a second mechanism in which a proton is donated from an internal group, as discussed above. Here, we considered AspL213 as a possible internal donor and started the simulation with the proton on this group. The results of the simulation are shown in Figure 9, in which it can be seen that it now takes ≈70 μs for the system to reach equilibration, when 50% of protons are transferred to Q_B. This transfer time is longer than that obtained in the first mechanism (Fig. 8). The longer time reflects the fact that SerL223 does not provide a pathway for a transfer to Q_B in the present structural model. The transfer from the AspL213 to Q_B probably requires that the proton will pass through W34 and will then overcome rate-limiting barriers, which probably are the same as those encountered in the first mechanism. Of course, the proton translocation in other structural models can be faster, and our results are valid only for the present set of protein coordinates. Thus, a more systematic study of this effect of structural changes is left to subsequent investigations.

The involvement of particular residues in the PT process can be tested by leaving them out or by introducing a high-energy barrier instead. This was tried here by arbitrarily setting the ΔG of AspL210 to 10 kcal/mol. The results are shown in Figure 10. The overall character of the curves is not altered much. However, the proton density at Q_B^- is higher, primarily because AspL210 is not available now as proton trap. The overall PT pathway is not changed.

CONCLUSIONS

This work developed a general method for simulating proton translocations in proteins. The method determines

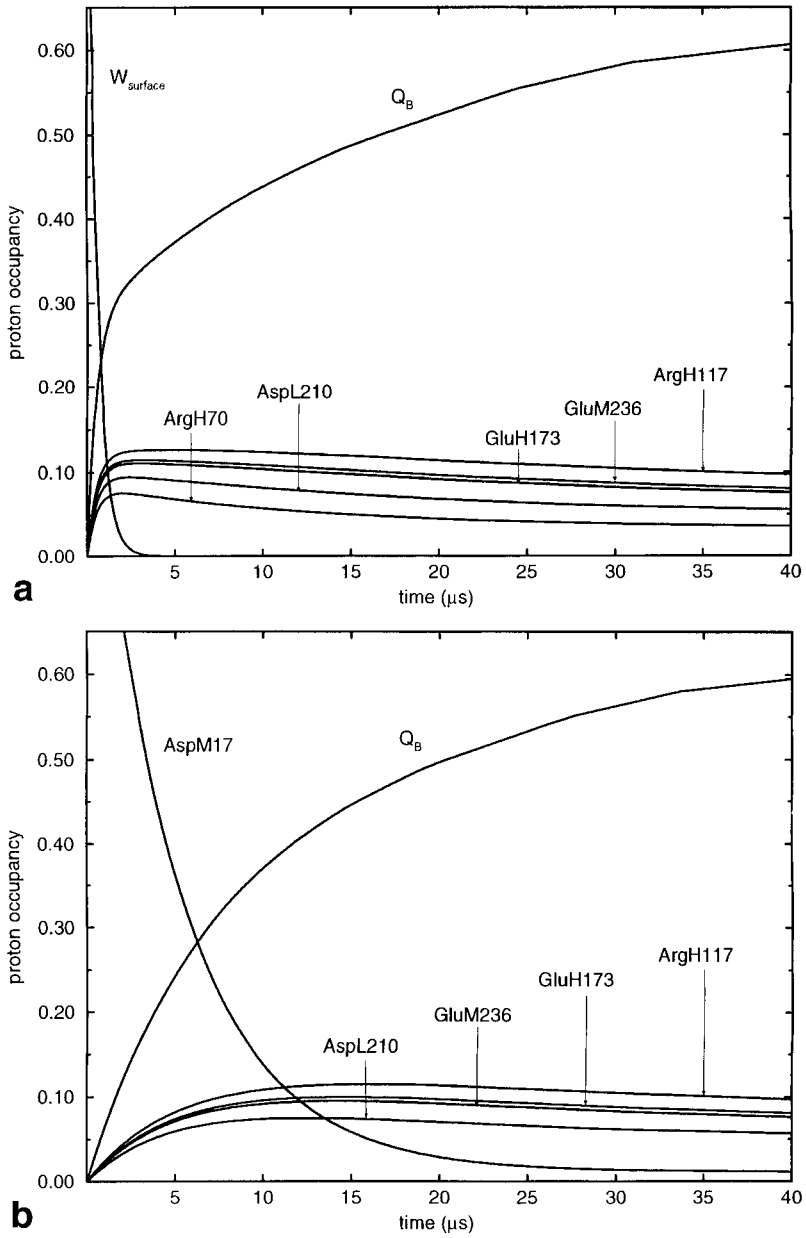

Fig. 8. The time evolution of the proton population starting with a proton placed on a surface water near W124 (**a**) and with a protonated surface water placed near AspM17 (**b**). The populations of all groups with proton occupancies >0.08% at any time during the simulations are shown. The population of $W_{surface}$ is not shown in b, because it becomes almost zero in 0.5 nanoseconds, and such a fast event cannot be described by the microsecond scale used here.

the rate constants for the individual PT steps by evaluating the relevant energetics using the PDLD/S approach and then using the Marcus-like HW expression to determine the relevant activation barriers and the corresponding rate constants. The time-dependent probability of finding the proton at different sites is then evaluated by using a master equation. Our method was demonstrated in this work by considering proton translocations across crystallographic water molecules and ionizable protein residues in the *Rhodobacter sphaeroides* reaction center. In doing so, we have not yet tried to solve mechanistic controversies or to identify with certainty the actual proton pathways. Instead, we focused on the methodological aspects and considered the calculated kinetics as the result of a preliminary study. Nevertheless, the simulations provide a significant insight into the nature of proton translocations in proteins. It was found that the free energy profile for the proton translocation is quite rugged (see, e.g., Fig. 7), reflecting the electrostatic interactions between the proton sites and their protein environments. These electrostatic effects involved both the intrinsic free energy of bringing a proton to a given site when all other

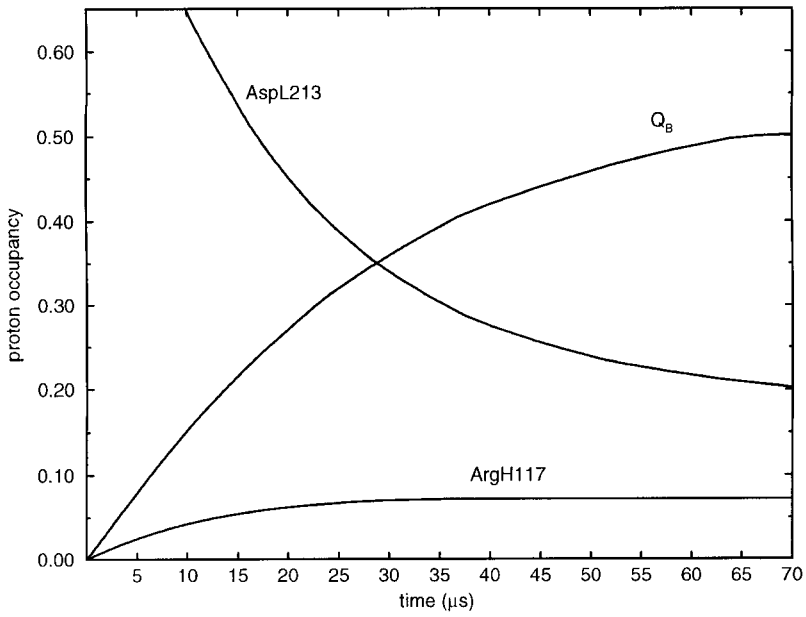

Fig. 9. The time evolution of the proton populations starting with a proton on AspL213.

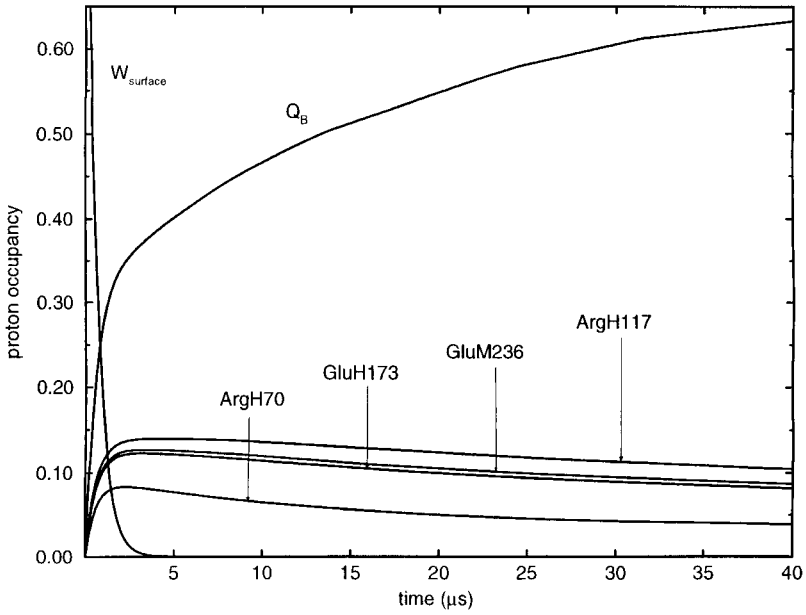

Fig. 10. The time evolution of the proton population starting with a protonated surface water near W124 and increasing the ΔG of AspL210 by 10 kcal/mol relative to its ΔG in the simulation shown in Figure 8.

sites are neutral and the free energy due to the interaction between the site and the charges of the surrounding sites. The energetics of the protonated sites [the $\Delta G^{(m)}$] appears to be the most important factor in determining the rate-determining barriers and the overall kinetics. In considering this point, we should not confuse the situation in proteins with the situation in bulk water or ice. That is, in the case of PT in water, the free energy ΔG^0 for each step is zero, and the activation barriers are close to zero.[24] In this case, the details of the rearrangement of the proton-conducting molecules is important in distinguishing between different mechanisms with different activation barriers (for example, one may want to distinguish between the Grotthuss mechanism[24,52] and other feasible mechanisms). However, although this may be quite interesting, the actual difference between the rate constants of the concerted and nonconcerted mechanisms in systems with $\Delta G^0 = 0$ for each step is quite small (smaller than 1 order of

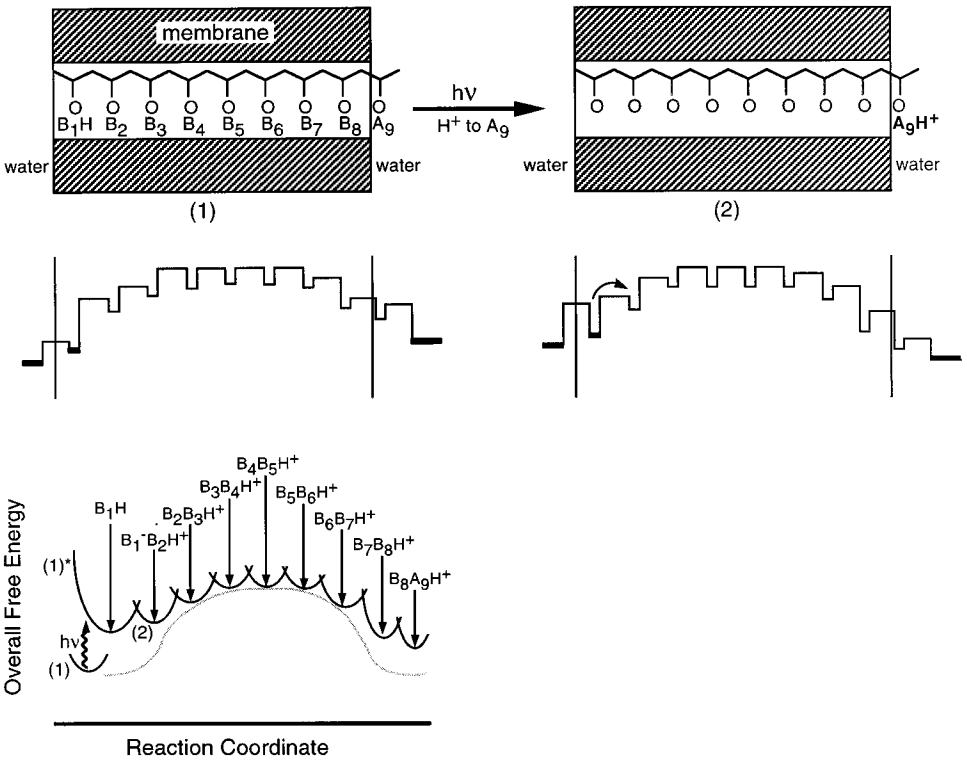

Fig. 11. The energetics of a hypothetical inefficient proton pump. The system is comprised of a chain of identical bases that would have the same pK_a in water. However, in the membrane, these pK_a values and the corresponding ΔG^0 values change drastically due to the dielectric barrier of the membrane. This leads to a high activation barrier for transferring the proton across the membrane. The top part of the figure describes the hypothetical system of bases. The middle part describe the proton energy on each site before and after the formation of A_9^-. The bottom part describes the total free energy in each step [$\Delta G^{(m)}$ in Eq. 2] and emphasizes the formation of a large barrier for the configuration in which the proton is in the center of the membrane. The light gray line designates the free energy of transferring a charge from water to the corresponding point in the membrane (for further discussion, see Warshe [11] and Warshel and Schlosser[54]).

magnitude). However, in proteins or in other heterogeneous environments, the barriers usually are higher than a few kcal/mol, and we can neglect their modifications by the internal rearrangements of the proton donors and acceptors (see Results, above). Thus, the effects of such internal rearrangements, which are the main feature of Nagel's model,[8] are of secondary importance relative to the effects of the environment on the activation barrier.[11]

The present study indicates that there are many alternative pathways for the proton translocations process. In some cases, it appeared that ionized protein residues play a major role in the transfer of protons between water molecules. Thus, the PT pathway is unlikely to only involve internal water molecules. Even if one finds in a protein a chain of water molecules that seems like a perfect 'proton wire,' it does not mean that the rate of proton transport is determined by the structure rearrangements of this wire or that this rate constant will be related to the corresponding rate constant in bulk water. Here again, as demonstrated in Figure 6, we probably will find that the interaction with the local environment leads to significant changes in the ΔG^0 of different steps, so that these free energies will determine the rate-limiting step. An instructive example can be provided by an attempt to design an artificial proton wire by inserting a chain of covalently linked bases (acids) of identical pK_a^w across a membrane or a hypothetical nonpolar protein (Fig. 11). Here, as discussed by Warshel,[11] we will find that ΔG^0 is controlled by the electrostatic energy of bringing the positively charged group from water to its specific site. Thus, the large free energy needed to bring a charge to a nonpolar region will determine the rate constant. The situation will be similar for a proton wire composed of a chain of water molecules that are inserted across a membrane or a hypothetical nonpolar protein. In that case, one might propose that a charge delocalization between several water molecules will reduce the electrostatic barriers. However, as demonstrated in EVB pictures of the type presented in Figure 5, the energy of the diabatic states in which the proton is localized on one site at the center of the membrane (e.g., H_2O H_3O^+ H_2O H_2O and H_2O H_2O H_3O^+ H_2O) will be raised to a very high energy. The mixing of these states by their interaction term (H_{ij} in Eq. 8), which is the source of the delocalization effect, would not compensate for the high energy of the diabatic states. Obviously, a real protein (which does not resemble at all a nonpolar membrane) can control the ΔG^0 by providing the proper polar environment and even can lead to $\Delta G^0 \cong 0$ for each step along the proton pathway. However, there is not

enough evolutionary pressure for this, because the PT process usually is not the rate-limiting step.

The dynamics of proton translocations can be simulated by less phenomenological approaches than the master equation treatment used here. In principle, one may try to study PT processes by using direct MD simulations. This requires an analytic representation of the relevant potential surfaces, and such a representation is provided by using the EVB method,[13] which has been very successful in detailed simulations of PT in solution[12,13,24,25] and in proteins.[12,13] Proton conductance along pathways with low barriers can be studied by running MD trajectories along the relevant EVB surfaces in their multiconfiguration (MC-EVB) version. However, cases with high barriers cannot be studied by direct simulations and require a FEP/umbrella sampling treatment.[12] The situation will become more complex when there are several high-energy barriers. Fortunately, the overall kinetics obtained from the FEP/umbrella sampling activation barrier is likely to be similar to the results of the present treatment. In general, when the rate of proton translocation is limited by a high-energy barrier (or barriers), we do not expect to obtain a major new insight from more involved treatments, such as direct simulations.

The current study was not aimed at determining the actual proton pathways in *Rhodobacter sphaeroides*, as discussed above. This probably should be done by using a more recent structure[5] that suggested several alternative pathways. The calculations also should consider all of the mobile water molecules within the protein cavities as possible candidate for the proton translocation process. Furthermore, probably, a more sophisticated kinetic treatment with a master equation (or a related treatment) that involves many protons should be used rather than the average distribution of a single proton. However, all of these improvements can be accomplished quite easily in the framework of the present approach. Also, it is clear that a more systematic determination of the nature of proton translocations in proteins should involve comparisons of the corresponding calculated and observed effects of mutations. Our method provides a general way of performing such studies, because it is easy to delete different residues from the calculations or simply to make them inaccessible to protons (see Fig. 10). Thus, we believe that experimental studies of proton translocations can be augmented in an effective way by simulation studies.

ACKNOWLEDGMENTS

The authors thank Prof. M. Okamura for critical discussions.

REFERENCES

1. Mitchel P. Coupling of phosphorylation to electron and hydrogen transfer by a chemi-osmotic type of mechanism. Nature 1961;191: 144–148.
2. Ermler U, Fritzsch G, Buchanan SK, Michel H. Structure of the photosynthetic reaction centre from *Rhodobacter sphaeroides* at 2.65 Å resolution: cofactors and protein-cofactor interactions. Structure 1994;2:925–936.
3. Kannt A, Lancaster RD, Michel H. The coupling of electron transfer and proton translocation: electrostatic calculations on *Paracoccus dentrificans* cytochrome C oxidase. Biophys J 1998;74: 708–721.
4. Henderson R, Baldwin JM, Ceska TA, Zemlin F, Beckman E, Downing K. Model for the structure of bacteriorhodopsin based on high-resolution electron cryo-microscopy. J Mol Biol1990;213:899–929.
5. Stowell MHB, McPhillips TM, Rees DC, Soltis SM, Abresch E, Feher G. Light-induced structural changes in photosynthetic reaction center: implications for mechanism of electron-proton transfer. Science 1997;276:812–816.
6. Okamura MY, Feher G. Proton transfer in reaction centers from photosynthetic bacteria. Ann Rev Biochem 1992;61:861–896.
7. Abresch EC, Paddock ML, Stowell MHB, McPhillips TM, Axelrod HL, Soltis SM, Rees DC, Okamura MY, Feher G. Identification of proton transfer pathways in the X-ray crystal structure of the bacterial reaction center from *Rhodobacter sphaeroides*. Photosyn Res 1998;55:119–125.
8. Nagel JF, Morowitz H. Theory of hydrogen bonded chains in bioenergetics. Proc Natl Acad Sci USA 1978;75:298–302.
9. Nagel JF, Mille M. Molecular models of proton pumps. J Chem Phys 1981;74:1367–1372.
10. Warshel A. Conversion of light energy to electrostatic energy in the proton pump of *Halobacterium halobium*. Photochem Photobiol 1979;30:285–290.
11. Warshel A. Correlation between structure and efficiency of light-induced proton pumps. In: Packer L, editor. Methods in Enzymology. London: Academic Press Inc., 1986; p. 578–587.
12. Åqvist J, Warshel A. Simulation of enzyme reactions using valence bond force fields and other hybrid quantum/classical approaches. Chem Rev 1993;93:2523–2544.
13. Warshel A. Computer modeling of chemical reactions in enzymes and solutions. New York: John Wiley & Sons; 1991.
14. Rabenstein B, Ullmann GM, Knapp EW. Energetics of electron-transfer and protonation reactions of the quinones in the photosynthetic reaction-center of *Rhodopseudomonas viridis*. Biochemistry 1998;37:2488–2495.
15. Beroza P, Fredkin DR. Electrostatic calculations of amino acid titration and electron transfer, $Q_A^- Q_B \rightarrow Q_A\, Q_B^-$. Biophysics 1995;68: 2233–2250.
16. Lancaster CRD, Michel H, Honig B. Calculated coupling of electron and proton transfer in the photosynthetic reaction center of *Rhodopsedomonas viridis*. Biophys J 1996;70:2479.
17. Sham YY, Chu ZT, Warshel A. Consistent calculations of pK_a's of ionizable residues in proteins: semi-microscopic and macroscopic approaches. J Phys Chem B 1997;101:4458–4472.
18. Warshel A. Calculations of enzymatic reactions: calculations of pK_a, proton transfer reactions, and general acid catalysis reactions in enzymes. Biochemistry 1981;20:3167–3177.
19. Bashford D, Karplus M. pK_a's of ionizable groups in proteins: atomic detail from a continuum electrostatic model. Biochemistry 1990;29:10219–10225.
20. Yang AS, Gunner MR, Sampogna R, Sharp K, Honig B. On the calculation of pK_a's in proteins. Proteins 1993;15:252–265.
21. Lee FS, Chu ZT, Warshel A. Microscopic and semimicroscopic calculations of electrostatic energies in proteins by the POLARIS and ENZYMIX programs. J Comp Chem 1993;14:161–185.
22. Sham YY, Muegge I, Warshel A. The effect of protein relaxation on charge-charge interactions and dielectric constants of proteins. Biophys J 1998;74:1744–1753.
23. Hwang J-K, Warshel A. How Important are quantum mechanical nuclear motions in enzyme catalysis? J Am Chem Soc 1996;118: 11745–11751.
24. Vuilleumier R, Borgis D. An Extended empirical valence bond model for describing proton transfer in $H^+(H_20)_n$ clusters and liquid water. Chem Phys Lett 1998;284:71–77.
25. Schmitt UW, Voth GA. Multistate empirical valence bond model for proton transport in water. J Phys Chem B 1998;102:5547–5551.
26. Hwang J-K, King G, Creighton S, Warshel A. Simulation of free energy relationships and dynamics of S_N2 reactions in aqueous solution. J Am Chem Soc 1988;110:5297–5311.
27. Warshel A, Russell ST. Calculations of electrostatic interactions in biological systems and in solutions. Q Rev Biophys 1984;17:283–421.
28. Press WH, Teukolsky SA, Vetterling WT, Flannery BP. Numerical

recipes in Fortran 77: the art of scientific computing, 2nd ed, volume 1. Cambridge: Cambridge University Press; 1992.
29. Alden RG, Parson WW, Chu ZT, Warshel A. Calculations of electrostatic energies in photosynthetic reaction centers. J Am Chem Soc 1995;117:12284–12298.
30. King G, Warshel A. A surface constrained all-atom solvent model for effective simulations of polar solutions. J Chem Phys 1989;91: 3647–3661.
31. Warshel A, Lappicirella A. Calculations of ground-and excited-state potential surfaces for conjugated heteroatomic molecules. J Am Chem Soc 1981;103:4664.
32. Eigen M. Proton transfer, acid-base catalysis, and enzymatic hydrolysis. Angewandte Chemie 1961;3:1–72.
33. Marcus RA, Sutin N. Electron transfers in chemistry and biology. Biochim Biophys Acta 1985;811:265–322.
34. Scheiner S. Proton transfers in hydrogen-bonded systems. Cationic oligomers of water. J Am Chem Soc 1981;103:315–320.
35. Scheiner S. Extraction of the principles of proton transfers by ab initio methods. In: Bountis T, editor. Proton transfer in hydrogen-bonded systems. New York: Plenum Press; 1992. p 29–47.
36. Marcus RA. Chemical and electrochemical electron transfer theory. Annu Rev Phys Chem 1964;15:155.
37. Lee FS, Warshel A. A local reaction field method for fast evaluation of long-range electrostatic interactions in molecular simulations. J Chem Phys 1992;97:3100–3107.
38. Tiede DM, Utschig L, Hanson DK, Gallo DM. Resolution of electron and proton transfer events in the electrochromism associated with quinone reduction in bacterial reaction centers. Photosyn Res 1998;55:267–273.
39. Hanson DK, Schiffer M. Symmetry-related mutants in the quinone binding sites of the bacterial reaction center—the effects of changes in charge distribution. Photosyn Res 1998;55:275–280.
40. Fritzsch G, Kampmann L, Kapaun G, Michel H. Water clusters in the reaction centre of *Rhodobacter sphaeroides*. Photosyn Res 1998;55:127–132.
41. Allen JP, Williams JC, Graige MS, Paddock ML, Labahn A, Feher G, Okamura MY. Free energy dependence of the direct charge recombination from the primary and secondary quinones in reaction centers from *Rhodobacter sphaeroides*. Photosyn Res 1998;55:227–233.
42. Nabedryk E, Breton J, Okamura MY, Paddock ML. Direct evidence of structural changes in reaction centers of *Rb. sphaeroides* containing suppressor mutations for Asp L213→Asn: an FTIR study of Q_B photoreduction. Photosyn Res 1998;55:293–299.
43. Paddock ML, Senft ME, Graige MS, Rongey SH, Turanchik T, Feher G, Okamura MY. Characterization of second site mutations show that fast proton transfer to Q_B^- is restored in bacterial reaction centers of *Rhodobacter sphaeroides* containing the Asp-L213→Asn lesion. Photosyn. Res. 1998;55:281–291.
44. Shinkarev V. The general kinetic model of electron transfer in photosynthetic reaction centers activated by multiple flashes. Photochem Photobiol 1998;67:683–699.
45. Miksovska J, Kalman L, Schiffer M, Maroti P, Sebban P, Hanson DK. In bacterial reaction centers, rapid delivery of the second proton to Q_B can be achieved in the absence of L212Glu. Biochemistry 1997;36:12216–12226.
46. Graige MS, Paddock ML, Bruce JM, Feher G, Okamura MY. Mechanism of proton-coupled electron transfer for quinone (Q_B) reduction in reaction centers of *Rb. sphaeroides*. J Am Chem Soc 1996;118:9005–9016.
47. Paddock ML, Rongey SH, Feher G, Okamura MY. Pathway of proton transfer in bacterial reaction centers: replacement of glutamic acid 212 in the L subunit by glutamine inhibits quinone (secondary acceptor) turnover. Proc Natl Acad Sci USA 1989;86: 6602–6606.
48. Miksovska J, Valerio-Lepiniec M, Schiffer M, Hanson DK, Sebban P. In bacterial reaction centers, a key residue suppresses mutational blockage of two different proton transfer steps. Biochemistry 1998;37:2077–2083.
49. Paddock ML, Rongey PH, McPherson AJ, Feher G, Okamura MY. Pathway of proton transfer in bacterial reaction centers: role of aspartate-L213 in proton transfers associated with reduction of quinone to dihydroquinone. Biochemistry 1994;33:734–745.
50. Takahashi E, Wraight CA. Proton and electron transfer in the acceptor quinone complex of *Rhodobacter sphaeroides* reaction centers: characterization of site-directed mutants of the two ionizable residues, GluL212 and AspL213, in the Q_B binding site. Biochemistry 1992;31:855–866.
51. Lancaster CRD. Ubiquinone reduction and protonation in photosynthetic reaction centres from *Rhodopseudomonas viridis*: X-ray structures and their functional implications. Biochim Biophys Acta 1998;1365:143–150.
52. Agmon N. The Grotthuss mechanism. Chem Phys Lett 1995;244: 456–462.
53. Kraulis PJ. MOLSCRIPT: a program to produce both detailed and schematic plots of protein structures. J Appl Crystal 1991;24:946–950.
54. Warshel A, Schlosser DW. Electrostatic control of the efficiency of light-induced electron transfer across membranes. Proc Natl Acad Sci USA 1981;78:5564–5568.